Brain Symmetry Plane Detection based on Fractal Analysis

S. A. Jayasuriya[*a], A. W. C. Liew[a], N. F. Law[b]

[a]School of Information and Communication Technology, Griffith University, Southport, QLD, 4222, Australia.

[b]Department of Electronic and Information Engineering,
The Hong Kong Polytechnic University, Hung Hom, Kowloon, Hong Kong.

Abstract

In neuroimage analysis, the automatic identification of symmetry plane has various applications. Despite the considerable amount of research, this remains an open problem. Most of the existing work based on image intensity is either sensitive to strong noise or not applicable to different imaging modalities. This paper presents a novel approach for identifying symmetry plane in three-dimensional brain magnetic resonance (MR) images based on the concepts of fractal dimension and lacunarity analysis which characterizes the complexity and homogeneity of an object. Experimental results, evaluation, and comparison with two other state-of-the-art techniques show the accuracy and the robustness of our method.

Keywords: Fractal Analysis, Lacunarity, Neuroimaging, Mid-sagittal Plane, Longitudinal Fissure.

[*]**Corresponding author Tel: +61 7 555 28502, Fax: +61 7 5552 8066**
Email addresses: **surani.jayasuriya@griffithuni.edu.au (S. A. Jayasuriya)**,
a.liew@griffith.edu.au (A. W. C. Liew), ennflaw@polyu.edu.hk (N. F. Law)

1. Introduction

Modern imaging techniques allow in vivo visualization of the brain providing vast amount of anatomical and functional information. Especially, the advent of high quality neurological MRI has the ability to produce three dimensional images with high soft tissue contrast. Precise clinical diagnosis and patient treatment can further be supported by quantitative image analysis techniques. However, despite the extensive research, visual interpretation is still the common method used in clinical practice [1]. Anatomical complexity of the brain has made automated brain image analysis a particularly challenging task.

A normal brain holds approximate bilateral symmetry. Highly convolved brain is separated into the left and right hemispheres by the inter-hemispheric fissure (IF) or the longitudinal fissure, which is a long and deep furrow (see Fig. 1). Although the real separation surface is not perfectly planar, the plane that passes vertically through this midline is considered to be the mid-sagittal plane (MSP) which also aligns with the plane dividing the body into two symmetrical parts. The symmetry plane of the brain is often considered as a first-order approximation to the MSP [2]. Knowing the precise location of the MSP is an important initial step in neuroimage analysis, and is of great interest in a number of medical applications. For example, it helps in identifying anatomical areas of interest for diagnosis, treatment and serves as a basis for asymmetry study of the brain [3]. MSP can bring multiple images into a common anatomical co-ordinate system like Talairach-Tournoux [4] thus reducing the degrees of freedom in multimodal registration of brain images. Usually, MSP is located manually by a neuroanatomy expert whose time is taken to process a massive number of scans. Moreover, manual methods suffer from operator dependency and the difficulty to

achieve accurate reproducibility. Therefore, a robust and accurate automatic technique to identify the MSP can be useful in clinical practice.

[Figure 1 about here.]

Despite the variety of methods being proposed, MSP detection remains a challenging issue due to the natural anatomical complexity, the presence of various noise artifacts [5, 6], pathologies, and tilted head scans. Most of the existing work has concentrated primarily on the image intensity analysis to detect the symmetry. However, it is the brain's structure itself which is symmetrical. To the best of our knowledge, none of the work on brain symmetry plane detection has tried to take advantage of the local self-similarity and bilateral symmetry in the structure present in brain images. Nevertheless, a recent work in [7, 8] assumes the MSP to be the plane that best partitions the external surface of the head into two symmetrical parts. The brain has a complex geometric structure which cannot completely be described using only measures based on Euclidean geometry [9]. Such complex geometry can however be characterized by fractal geometry. Fractal dimension (FD) provides a way of quantifying the shape complexity of objects. Fractal analysis has already been successfully used in various areas such as mathematics, science, biology and medicine. The use of a fractal dimension to describe the convolution or the complexity of a line or surface is well established in several areas of biomedical research [10].

In this paper, as the sequel of our previous work [11], we focus on detecting the MSP of the brain based on the fractal features of the textures present on neurological MRI. In our previous work, we proposed using fractal dimension as a symmetry measure for detecting MSP. The idea behind our approach is based on the assumption that the left and right hemispheres would be similar in structural complexity. In this paper, we exploit both fractal dimension and lacunarity for locating the MSP of three-dimensional (3D) brain volumes. We also carried out extensive experiments to test the viability of a fractal based method in MSP

detection. Our results show that the method is robust to noise, applicable to different imaging modalities and is able to handle pathological cases. The method can also be applied on 2D axial or coronal scans.

2. Related Work on MSP Detection

A number of papers have tackled the brain symmetry plane estimation problem. A review can be found in [12]. These methods can be categorized based on two main approaches. The first approach ([13]-[16]) is to detect some anatomical feature like IF to estimate the location of MSP. In the method by Bergo et al. [15], it is assumed that IF contains the maximum area of CSF when ventricles are excluded. By creating a 3D brain mask that excludes ventricles, the CSF score of each sagittal plane is obtained by computing the mean voxel intensity in the intersection between the plane and the brain mask. The plane with a reasonably large brain mask intersection and minimal intensity score is taken as the best candidate for the MSP. Then, the CSF score is again calculated for all small transformations of the chosen plane and the plane with the lowest score is considered to be the MSP.

Volkau et al. [14] proposed another impressive method using Kullback-Leibler (KL) Divergence. They assume that the entropy of MSP is lower than that of the neighbouring sagittal slices due to its large amount of cerebrospinal fluid (CSF). Let the probability distributions of the intensities of two sagittal slices be given by $P = \{p_i\}$ and $Q = \{q_i\}$, KL divergence measure is defined as

$$\begin{aligned} D_{KL}(p \parallel q) &= \sum_i p_i \log(p_i) - \sum_i p_i \log(q_i) \\ &= \sum_i p_i \log(p_i / q_i) \end{aligned} \qquad (1)$$

In their method, a volume of interest (VOI) is defined around the central slice in the sagittal direction and the KL measure is computed on all sagittal slices comparing each to the

first slice of the VOI. By taking the slice that gives the maximum KL measure as the central plane for a new smaller VOI, a new search is performed until finally the MSP is estimated.

Methods in the first category are generally insensitive to pathological asymmetry. However, most of them are hard to extend to different imaging modalities and can be sensitive to noise and outliers. Existing methods also have some restrictions regarding the search area. Some prior assumption or knowledge about the approximate location of the MSP is needed to obtain good result.

The second approach defines MSP as a plane that maximizes the similarity of the two brain hemispheres [17]-[20]. Since brain is not perfectly symmetrical, several measures that quantify the degree of similarity between the two hemispheres have been proposed in the literature. Most of the work uses intensity based cross correlation. Cross correlation cc between two images P and Q can be calculated as

$$cc = \frac{\sum_i (P_i - \overline{P})(Q_i - \overline{Q})}{\sqrt{\sum_i (P_i - \overline{P})^2}\sqrt{\sum_i (Q_i - \overline{Q})^2}} \qquad (2)$$

where P_i and Q_i are the intensity values in the ith pixel and $\overline{P}$ and $\overline{Q}$ are the respective means of the entire image.

Usually, the image is reflected across the estimated plane and the cc is measured between the original and the reflected images. The more recent edge based cc method [17], [21] is different from the traditional intensity based cc technique in that it performs the cross correlation on an edge image in order to capture the anatomical structures of the brain and skull while ignoring intensity fluctuations. Although the method is capable of finding the MSP accurately on certain pathological images, the results could severely get affected by the initial estimate of the MSP computed on a lower brain slice, and the orientation of the image.

Methods in this second category can easily be extended to different imaging modalities. However, besides being computationally demanding, intensity based reflection approach is

highly sensitive to the asymmetry caused by pathologies because of the similarity criterion used.

Despite the variety of work done in addressing the issue of MSP detection, there is still no method commonly accepted as the best. For an algorithm to be used in clinical practice, it has to be fast, robust and accurate [6], [13]. Existing techniques leave significant room for applicability and accuracy. The closest related work to our approach is the method proposed by [14], mentioned above. Although the approach gives good results in many cases, in our simulations it did not perform well on images with lower resolution or large amount of noise.

3. Fractal Analysis in Medical Applications

Since Mandelbrot [22] first introduced the concept of fractals for describing the complexity of an object, fractal analysis has been widely applied to various scientific areas, including medical imaging [23]. Fractal dimension (FD) contains information about the geometric structures of fractals. Many natural structures exhibit self-similarity over a range of scales, enabling them to be described by a fractal dimension. Since medical images are complex in nature and exhibit some similarity in different scales, fractal geometry has been applied in analysing a variety of medical images, and has played an important role in various areas of health and medical research such as differentiating pathological tissues from healthy ones [24-25] and diagnosis in a broad range of diseases [26]. It has also been successfully used in quantification of morphological changes in brain images [10].

The choice of fractal analysis on medical imaging is also motivated by the observation that FD is relatively insensitive to image scaling, and it shows a strong correlation with human judgment of surface roughness [27]. Moreover, FD has been shown to be a powerful tool for quantitative characterization of noisy medical images where the edges are usually blurred, and diagnostically important information usually lies in the texture [28].

4. Materials and Methods

4.1. Fractal Analysis

A fractal is defined as a fragmented geometric shape that can be divided into smaller parts, where each part is a smaller copy of the whole [22]. This is an important property of the fractal called self-similarity (see Fig. 2). Several of the best known examples of mathematical fractals are the Koch curve, the Sierpinski gasket and the Cantor set.

[Figure 2 about here.]

Some of the basic concepts of fractals can be elucidated with the Koch curve which has much of the complexity that we would see in natural objects (see Fig. 2 (b)). Its construction is an iterative procedure, beginning with a straight line segment called the initiator. The initiator is partitioned into three equal segments and then the middle segment is replaced by two equal segments, forming an open equilateral triangle. This completes the basic construction step which is called the generator. Then, the procedure is repeated for every straight line segment, and in theory, the process can be continued to infinity. The result is neither a curve nor a surface but rather an infinite curve that fills the surface [29]. Each sub-segment is an exact replica of the original curve, thus showing the self-similarity.

When measuring the total length of the Koch curve, the result depends on the length of the scale. This leads towards a definition of the fractal dimension, related to the number of self-similar pieces that can be seen when scaling down a larger object.

4.1.1. Fractal Dimension

FD can quantify the complexity of an object, indicating how much space is filled with increasing scale [22]. FD is a real number that describes the structural complexity of an object. It is defined as the exponent of the number of self-similar pieces (N) with

magnification factor (1/*r*) into which an object may be broken. The equation can be written as follow.

$$FD = -\frac{\ln N}{\ln r} \qquad (3)$$

FD can be obtained using least-squares linear regression to estimate the slope of the log-log plot of *N* versus 1/*r*.

In the case of the Koch curve, we could observe that at each step, the length of the curve grows by factor of 4/3. By decreasing the radius to one third, the measurable length *N* increases by a factor of four. Therefore, the fractal dimension in the case of the Koch curve is

$$FD = \ln(4)/\ln(3) = 1.2618$$

For a truly fractal structure the slope of the log-log graph is independent of the scale at which we observe the structure. When applying the concept of fractals to biological structures, we merely expect it to be approximately constant within some range of scale. Fig. 3 shows a log-log plot obtained from a 3D brain MR image. FD is obtained by fitting a straight line to the plot using least square regression.

[Figure 3 about here.]

4.1.2. Lacunarity

When Mandelbrot [22] introduced the fractal geometry, he defined and used the concept of lacunarity as another complementary metric which describes the deviation from homogeneity in the texture [30]. Its initial purpose was to further classify fractals and textures which had the same fractal dimension but very different visual appearance. Lacunarity, from the Latin word lacuna meaning “gap” describes the texture of an object by measuring the degree of non-homogeneity within an object or image (see Fig. 4). If an object has large holes or gaps distributed unevenly, it has high lacunarity. On the other hand, if an object is

homogeneous with respect to the spatial arrangement of gaps or almost translationally invariant, it has low lacunarity. This is defined quantitatively as the mean square deviation of the fluctuation of mass distribution function divided by its square mean [31-32].

Lacunarity has been taken as a quantitative measure of texture in various fields [33-34]. In [35], Zaia et al. presented a method based on lacunarity analysis for studying trabecular bone structure to differentiate healthy and osteoporotic patients.

[Figure 4 about here.]

4.2. Motivation

In the work by Kiselev et al. [36], an analysis of the geometry of the human cerebral cortex has been performed over all spatial scales and it is shown that the cortex does possess some self-similarity. Free et al. [10] have studied the fractal dimension of the white matter surface from MRI and found that FD for each hemisphere is remarkably similar. They have also mentioned that there was no significant correlation between the surface area of a region or block and the fractal dimension of that region, indicating that the fractal dimension measure some other feature of objects like the complexity across a range of scales.

Our approach is based on the assumption that both left and right hemispheres have similar FD. Once the 3D brain is divided into two parts in the sagittal direction, the difference of FD of the two parts should be at a minimum when the division is chosen to be at the MSP. Fig. 5 (A) demonstrates the log-log plots taken at any random sagittal location which is not MSP (left image) and at the MSP ground truth (right image). At the location of the ground truth, the left and right plots nearly coincide.

It is shown that two objects with the same fractal dimension can be different in appearance [33]. Lacunarity has the ability to differentiate this. Even small differences in texture can result in measurably different lacunarity values [34]. In our experiments we found that the average lacunarity value of the MSP was greater than the immediate neighbouring slices (see

Fig. 5 (B)). However, using maximum lacunarity alone was not reliable enough, especially for images with pathology or strong noise due to its sensitivity to these factors. Hence, our approach combines both FD and lacunarity for the robust estimation of the MSP.

4.3. Procedure

Based on the observation that the FD difference between the left and right hemispheres would be at a minimum for the MSP, we define a new symmetry criterion. Let the FD of the whole image, the left part, and the right part be denoted as FD_W, FD_L, and FD_R, respectively, our symmetry measure α is defined by

$$\alpha = \frac{\left|FD_L - FD_R\right|}{FD_W} \qquad (4)$$

In practice, the estimation of the FD for a real object by a direct application of the FD formulae is not always possible. Natural objects are not regular and are self-similar only in a statistical sense. Therefore, various methods have been put forward for the determination of the FD, each having its advantages and disadvantages in terms of accuracy or required computation time. The box-counting method [37] is the most widely used method to compute the fractal dimension due to its power in representing structural complexity and its easy implementation [38]. In our work, we used this box-counting fractal dimension.

4.3.1. The box-counting method

In this method, the object to be analysed is covered with 3D boxes, each of side length *r*. At each step of the procedure, the linear size *r* is changed to progressively smaller sizes. The minimum number of boxes N(r) that is necessary to cover the whole object structure is then assumed to vary according to $N(r) \sim (1/r)^{FD}$, where *FD* is the fractal dimension. We plot a

log-log plot of $N(r)$ versus r, and then fit a straight line to the plotted points. The measure of the slope gives us the Box-counting fractal dimension.

4.3.2. Estimate of lacunarity

In the BC method, lacunarity λ is calculated [31, 39] from the mean (μ) and the standard deviation (σ) of the number of pixels within the boxes of side length r as

$$\lambda(r) = \frac{\sigma_r^{\,2}}{\mu_r^{\,2}} \qquad (5)$$

Specifically, a box of size r is placed over the top left corner of the image, and the box mass (average intensity values) is calculated. Then, the box is moved along the row and column directions, and the box mass is computed again. After repeating this process over all rows and columns, a frequency distribution of the box masses can be obtained. The frequency distribution can be converted to a probability distribution by dividing by the total number of boxes. Using the first and second moments of this distribution, Lacunarity for that box size r could be computed.

4.3.3. Algorithm

1: Read 3D brain data $I(x; y; z)$. X, Y, Z be the left-right, anterior-posterior and top-bottom axes, respectively.

2: Estimate the FD, FD_W for whole image.

3: Select the sagittal region Ω of the image I by ignoring the extreme 20% end slices.

4: For each sagittal location c in the region Ω

- Estimate the FD, FD_L for the portion of Ω to the left of c.
- Estimate the FD, FD_R for the portion of Ω to the right of c
- Compute α(c) by eqn. (4) using FD_W, FD_L, and FD_R.

5: By considering all candidate planes, find the c^* that gives the minimum α.

6: Assign c^* to be an estimate for the sagittal location for MSP.

To refine the estimated MSP position using lacunarity:

7: Consider a region of interest (ROI) centred on c^* , and select sagittal planes s within the ROI centred on $c^* \pm \delta$. When creating these planes, only the coordinate in the sagittal direction is changed while keeping the other two co-ordinates similar to those of c^*. So, if the co-ordinates of c* can be given as (c^*,y^*,z^*), co-ordinates of the candidate planes will be (s,y^*,z^*), where $s \in [c^* \pm 1]$. We took δ as 0.5mm.

8: Compute the average lacunarity values λ_s for the chosen planes s. The average lacunarity is obtained by taking the mean of the lacunarity values for all boxes of side length r.

9: By considering all candidate planes within the ROI, find the s_0 that gives the maximum average value for λ.

10: Assign s_0 to be the sagittal location for MSP.

When applying the method on axial or coronal 2D images (in a case that the test image is 2D as in Figure 12 phantom brain), computing α is straightforward. When calculating lacunarity, small rectangular regions within the ROI were considered.

Before implementing the method on brain MRI, it was validated by using simulated images with a known fractal dimension. As shown in Fig. 6, the computed FD was close to the true or theoretical value, showing the reliability of the method. Fig. 6 (b) also validates our symmetry measure.

[Figure 6 about here.]

5. Results

5.1. Data Overview

The MR image datasets were provided by the Centre for Morphometric Analysis at Massachusetts General Hospital and is available at http://www.cma.mgh.harvard.edu/ibsr/ [40]. Datasets from AANLIB (http://www.med.harvard.edu/) [41], and BrainWeb (http://www.bic.mni.mcgill.ca/brainweb/) [42] databases were also used for analysing the robustness of the method. A total of 104 MR scans (see Table 1) of normal and pathological cases in T1-, T2- and PD-weighted images were included in the dataset. Simulated data from BrainWeb were used to analyse the effect of noise and intensity non-uniformity. The size of each 3D image was 256x256xZ (Z varied from 60 to 64) for IBSR data and 181x217x181 for BrainWeb simulated images. AANLIB images were 256x256 2D images. The robustness of the algorithm to the modality (T1, T2 and PD) of the image was also checked. The slice thickness varied between 1mm and 9 mm.

[Table 1 about here.]

Fig. 8 and Fig. 9 illustrate sample results obtained projected on the axial or coronal slices. Fig. 8 shows some of the results for the clinical images that include both normal and pathological images obtained from IBSR, AANLIB, and other clinical images. In order to analyse the effect of noise, INU, slice thickness, and modality; simulated images from BrainWeb were chosen and these results are shown in Fig. 9.

[Figure 7 about here.]
[Figure 8 about here.]
[Figure 9 about here.]

5.2. Visual Evaluation

The results were visually assessed by a medical doctor and were judged to be consistently correct. As can be seen in Fig.9, the accuracy of our method does not get affected by noise, INU, and different imaging contrasts. This could be understood as both left and right ROIs considered are affected by nearly equal amounts of noise and INU thus cancelling their

effects. Our method gives good results in pathological cases as well. We postulate that this is because in the pathological brain the abnormality resides only in a localized area and it does not affect the overall results of our box-counting FD estimation method.

5.3. Quantitative Evaluation

[Figure 10 about here.]

In order to compare our method with human performance we got the ground truth MSPs manually marked by a medical expert on 15 2D axial slices randomly taken from 5 MR images from IBSR data. Then, we measured the angular deviation (θ, in degrees) and average deviation of the distance (d, in pixels) of the end points between the estimated MSPs and the ground truth lines according to Fig. 7 and Eq.6. Summary of the results is shown in Table 2.

$$d = \frac{\sqrt{(xt_g - xt_e)^2 + (yt_g - yt_e)^2} + \sqrt{(xb_g - xb_e)^2 + (yb_g - yb_e)^2}}{2} \quad (6)$$

[Table 1 about here.]

We also compared our method with two state-of-the-art techniques: cross-correlation ([17], [19-21]) and KL-divergence measure ([14], [43]). These were implemented according to [17] and [14], respectively. Some of the comparison results are shown in Fig. 10.

[Figure 10 about here.]

To perform a quantitative comparison, we used 34 images from the BrainWeb database, and measured the average deviation d (in pixels) along the sagittal direction. Since the simulated images we considered were centred, and all of these methods gave a result in sagittal direction, there was no need to calculate the angle deviation. In order to compare the mean computational time, all methods were executed on the same machine (Intel Core2 duo

CPU p8700 2.53GHz 3.45GB RAM). The proposed method took 3 minutes for a 181x217x181 image. These results are summarized in Table 3. Even the fractal dimension alone in our method gave very good results, once refined using lacunarity, the method gave very accurate results most of the time.

[Table 2 about here.]

A paired t-test was performed to reveal the statistically reliable difference between the mean value of our method and that of the other two methods. The comparison results with the edge based cc method and the KLD method for the probability value for a 95% confidence level are shown in Table 4. These results indicate that we have a statistically significant lower mean value.

[Table 3 about here.]

5.4. Performance in pathological images

The robustness of the algorithm to pathological images was checked using 6 tumor images with progressive history taken from IBSR data. For each image of size 256x256x28, average pixel deviation from the ground truth was measured. Fig. 11-(i) shows a comparison with the two state-of-the-art techniques. Although the accuracy is affected by the severity of the pathology, in comparison with the two existing methods, our method performs well as its maximum deviation with the ground truth was only 2.5 pixels. Fig. 11-(ii) shows the best and worst case scenario of each method. Although the edge based method gives excellent results on simulated images with artificial tumors, the method performed poorly in the real images we tested here. The edge based method relies on the initial estimate taken from a lower brain axial slice. In its least performed image, the initial estimate gives incorrect results, thus severely affecting the final results. KLD method performs better in most cases, but still is sensitive to the changes due to pathology as the maximum KLD appears to be at a location different to the MSP's in those poorly performed images.

[Figure 11 about here.]

5.4. Tolerance to Noise

In order to measure the tolerance to noise, we made a comparison of the performance of these different techniques on an image with varying Gaussian noise. For this, we used the Shepp-Logan phantom image [44] which is a well-known standard imitation of the human brain. For the cross correlation technique we considered both the intensity based CC and the edge based CC methods. For the edge based CC method, we used the canny edge detector as mentioned in [17]. As the KLD technique and the edge based CC technique fail to locate the accurate symmetry plane in the noise free Shepp-Logan phantom image (see Fig. 12-(i) (a)), we modified the Shepp-Logan image by changing the contrasts of the ellipses in the middle of the image to a darker value (see Fig. 12-(i) (b)), so that all methods performed equally well in the noise-free image. We did this modification in this way as the edge based method relies on the initial edge image and the KLD method assumes that the maximum KLD occurs at a sagittal slice in the region of 20 mm apart from the medial slice. When this change is done on the image, the edge image showed the structures in the middle better and the maximum KLD occurred at the midline position.

Plots in Fig. 12-(i) demonstrate the performance of each method. 30 samples were used for each noise level tested. Since the deviation of our method from the ground truth was zero all the time, it is not visible in the plot. KLD method deviates from the ground truth as it is quite difficult to identify the mid-plane when there are multiple positions with maximum KLD, especially in a noisy image. Both cross correlation methods get affected by noise as they consider intensity/edge based similarity between the two sides. The fractal method, on the other hand, gives excellent results as the technique does not depend on the image intensity itself, but rather it measures the complexity of organization of image pixels. Fig. 12-(ii) shows the results obtained when each of these methods was applied on another phantom brain image with gradient and noise taken from IBSR database.

[Figure 12 about here.]

6. Discussion

Our analysis showed that the estimation of MSP in MR brain scans by means of fractal analysis is highly robust and accurate. Our method uses FD and lacunarity to locate the MSP as FD alone may not completely characterize the differences. It is possible that two objects can have the same fractal dimension, but different looks. In such cases, lacunarity becomes helpful in differentiating objects with the same FD values. During our experiments, in many cases we saw that MSP had maximum average lacunarity value in comparison with the other sagittal slices. However, lacunarity alone was not sufficient; especially in pathological or noisy images as average lacunarity value can be sensitive to these factors. Our method combining lacunarity and fractal dimension was able to give very accurate results.

There are various methods to compute FD besides box-counting. We have also experimented with differential box-counting method (DBC) [45]. Besides being computationally more expensive, it was not robust in the presence of strong noise. Brain structure can also be regarded as a mixture of different fractals [28]. In that case, multifractal analysis can give the distribution of the fractal dimension. However, for our purpose, the inexpensive box-counting method gives good results.

6.1. Advantages of a fractal analysis based method over existing techniques

As mentioned in Section I, a distinct feature of the brain are local self-similarity and the structural similarity of the two hemispheres. However, surprisingly, existing work has not taken advantage of these properties. Most of them either consider cross correlation as a symmetry measure or assume that the MSP contains a higher amount of CSF that can be distinguished in a neuroimage. These two approaches suffer from several shortcomings. First, as mentioned previously, the common procedure in the cross correlation technique is to

reflect the image across the estimated plane and to measure the CC between the original and the reflected image. This is a computationally demanding process and the result can easily be affected by the normal or abnormal hemispheric asymmetry. In MRI, artifacts like intensity non-uniformity (INU) give rise to smooth intensity variation across the image which can have a major impact on such intensity based methods [5-6]. Although the CSF appears dark in T1-weighted images, on other imaging modalities it appears differently. Ventricles which have a large amount of CSF and the contrast of pathologies on the image can affect the accuracy of a method which assumes that MSP has the maximum amount of CSF. Furthermore, these methods can also get affected by strong noise and low image resolution.

There are several advantages of using a fractal based method in brain MSP detection. First, as mentioned in previous sections, fractal geometry is well recognized for having the ability to capture the structural complexity of an object. Second, its scale invariance property allows it to perform well on images with different resolutions or strong noise. The computed log-log plots of images with different noise (see Fig. 13) demonstrate the noise resistance property of our fractal method. Moreover, as discussed earlier, since our method compares the structural similarity of left and right hemispheres which are affected by nearly equal amounts of noise and INU, results does not get affected by such artifacts.

[Figure 13 about here.]

6.2. Limitations of the proposed method

Although our method was robust to pathological images in comparison with the other existing techniques, the proposed algorithm still requires a certain degree of symmetry between the left and right hemispheres. Therefore, it may not give accurate results on images with severe global asymmetry like substantial hemispheric removal. However, this is also a limitation for all correlation based techniques. A possible direction for future research is to incorporate shape information in order to increase the robustness to pathology [7].

Since our method needs sagittal scans, if the initial orientation is either axial or coronal, we have to first get the sagittal slices. For instance, if we have axial scans and the head tilt is large, we have to get an initial estimate of the rotation angle. For this we used another method we have developed previously [16] to estimate large tilt angle. Then, we can generate sagittal slices taking into account the estimated tilt angle and apply our method to accurately detect the MSP.

As mentioned in Section I, the MSP detected as a straight line or a plane has numerous applications. However, MSP or IF is not exactly planar. It might be advantageous if the non-planar surface that separates the two hemispheres could be detected [46]. Although [47, 48] has started working on this direction, application to this particular problem of MSP detection has not been fully addressed yet. A possible future work is to extend the fractal based method for detecting non-planar MSP.

7. Conclusion

We have used fractal geometry for estimating the location of MSP in 3D MR images. The method incorporates both fractal dimension and lacunarity for robustness and precision. A symmetry measure was defined based on the assumption that the two brain hemispheres which are structurally similar would have similar fractal features. The implementation is simple without the need for any pre-processing like removal of skull. The method was extensively tested on various 3D MR images in different imaging modalities. Excellent results were obtained. The method is robust with respect to strong noise, intensity non-uniformity and pathology in the brain. Moreover, it works well on images with low resolution. It can also readily be used in different imaging modalities. In our future work, we plan to use the location of MSP for asymmetry analysis of pathological brains.

Acknowledgment

This work was supported by the Australian Research Council (ARC) Discovery Grant DP1097059 and the Australian Postgraduate Award (APA). We also thank Gold Coast Hospital for providing us with the clinical images.

References

[1] Hahn HK. Computer-assistance in neuroimaging: From quantitative image analysis to computer-aided diagnosis. In: IEEE International Symposium on Biomedical Imaging: From Nano to Macro. Rotterdam; 2010. p. 275–275.

[2] Kruggel F, von Cramon D. Alignment of magnetic resonance brain datasets with the stereotactical coordinate system. Medical Image Analysis. 1999;3(2):175–185.

[3] Fieten L, Eschweiler J, de la Fuente M, Gravius S, Radermacher K. Automatic extraction of the mid-sagittal plane using an ICP variant. In: Medical Imaging 2008: Visualization, Image-guided procedures, and Modeling. vol. 6918; 2008.

[4] Talairach J, Tounoux P. Co-Planar Stereotaxic Atlas of the Human Brain: 3-D Proportional System: An approach to cerebral imaging. New York: Thieme Medical; 1988.

[5] Liew AWC, Yan H. An adaptive spatial fuzzy clustering algorithm for MR image segmentation. IEEE Transactions on Medical Imaging. 2003;22(9):1063–1075.

[6] Liew AWC, Yan H. Current methods in the automatic tissue segmentation of 3D magnetic resonance brain images. Current Medical Imaging Reviews. 2006;2(1):91–103.

[7] Liu SX, Kender J, Imielinska C, Laine, A. Employing symmetry features for automatic misalignment correction in neuroimages. J Neuroimaging, 2011;21(2) 15-33.

[8] Liu SX, Imielinska C, Connolly Jr S, Ambrosio, AD. Automatic correction of the 3D orientation of the brain imagery. In: IEEE International Symposium on Signal Processing and Information Technology; 2006.

[9] Uemura K, Toyama H, Baba S, Kimura Y, Senda M, Uchiyama A. Generation of fractal dimension images and its application to automatic edge detection in brain MRI. Computerized Medical Imaging and Graphics. 2000;24:73–85.

[10] Free S, Sisodiya S, Cook M, Fish D, Shorvon S. Three-dimensional fractal analysis of the white matter surface from magnetic resonance images of the human brain. Cerebral Cortex. 1996;6(6):830–836.

[11] Jayasuriya SA, Liew AWC. Fractal dimension as a symmetry measure in 3D brain MRI analysis. In: IEEE International Conference on Machine Learning and Cybernetics; 2012.

[12] Liu SX. Symmetry and asymmetry analysis and its implications to computer-aided diagnosis: A review of the literature. Journal of Biomedical Informatics. 2009;42:1056–1064.

[13] Hu Q, Nowinski W. A rapid algorithm for robust and automatic extraction of the midsagittal plane of the human cerebrum from neuroimages based on local symmetry and outlier removal. NeuroImage. 2003;20:2153–2165.

[14] Volkau I, Bhanu P, Ananthasubramaniam A, Aziz A, Nowinski W. Extraction of the midsagittal plane from morphological neuroimages using the Kullback-Leibler's measure. Medical Image Analysis. 2006;10:863–874.

[15] Bergo F, Falcao A, Yasuda C, Ruppert G. Fast, accurate and precise mid-sagittal plane location in 3D MR images of the brain. Biomedical Engineering Systems and Technologies: Communications in Computer and Information Science. 2009;25:278–290.

[16] Jayasuriya SA, Liew AWC. Symmetry plane detection in neuroimages based on intensity profile analysis. In: IEEE International Symposium on Information Technology in Medicine and Education (ITME). vol. 2; 2012. p. 599–603.

[17] Liu Y, Collins R, Rothfus W. Robust Midsagittal plane extraction from normal and pathological 3-D neuroradiology images. IEEE Transactions on Medical Imaging. 2001;20(3):175–192.

[18] Thirion JP, Prima S, Subsol G, Roberts N. Statistical analysis of normal and abnormal dissymmetry in volumetric medical Images. In: IEEE Workshop on Biomedical Image Analysis; 2000. p. 74–83.

[19] Prima S, Ourselin S, Ayache N. Computation of the mid-sagittal plane in 3D brain images. IEEE Transactions on Medical Imaging. 2001;21:122–138.

[20] Tuzikov A, Colliot O, Bloch I. Evaluation of the symmetry plane in 3D MR brain images. Pattern Recognition Letters. 2003;24:2219–2233.

[21] Ruppert G, Teverovskiy L, Yu C, Falcao A, Liu Y. A new symmetry-based method for mid-sagittal plane extraction in neuroimages. In: IEEE International Symposium on Biomedical Imaging: From Nano to Macro. Chicago; 2011. p. 285–288.

[22] Mandelbrot B. The fractal geometry of nature. W.H. Freeman and Company; 1982.

[23] Lopes R, Betrouni N. Fractal and multifractal analysis: A Review. Medical Image Analysis. 2009;13:634–649.

[24] Blackledge J, Dubovitskiy D. Object detection and classification with applications to skin cancer screening. ISAST Transactions on Intelligent Systems. 2008;1(2):34–45.

[25] Takahashi T, Kosaka H, Murata T, Omori M, Narita K, Mitsuya H, et al. Application of a multifractal analysis to study brain white matter abnormalities of schizophrenia on T2-weighted magnetic resonance imaging. Psychiatry Research Neuroimaging. 2009;171:177–188.

[26] Iftekharuddin K. Techniques in fractal analysis and their applications in brain MRI. Medical imaging systems: technology and applications, Analysis and Computational Methods. 2005;1:63–86.

[27] Chaudhuri B, Sarkar N. Texture segmentation using fractal dimension. IEEE Transactions on Pattern Analysis and Machine Intelligence. 1995;17(1):72–77.

[28] Oczeretko E, Jurgilewicz D, Rogowski F. Some remarks on the fractal dimension applications in nuclear medicine. In: Fractals in Biology and Medicine. vol. 3; 2002.

[29] Sandu A, Rasmussen I, Lundervold A, Kreuder F, Neckelmann G, Hugdahl K, et al. Fractal dimension analysis of MR images reveals grey matter structure irregularities in schizophrenia. Computerized Medical Imaging and Graphics. 2008;32:150–158.

[30] Pentland A. Fractal-Based description of natural scenes. IEEE Transactions on Pattern Analysis and Machine Intelligence. 1984;6(6):661–674.

[31] Allain C, Cloitre M. Characterizing the lacunarity of random and deterministic fractal sets. Physical Review A. 1991;44(6):3552–3558.

[32] Tolle C, McJunkin T, Gorsich D. An Efficient implementation of the gliding box lacunarity Algorithm. Physica D. 2008;237:306–315.

[33] Taguchi Y. Lacunarity and Universality. J Phys A: Math Gen. 1987;20:6611–6616.

[34] Dougherty G, Henebry G. Fractal signature and lacunarity in the measurement of the texture of trabecular bone in clinical CT images. Medical Engineering and Physics. 2001;23:369–380.

[35] Zaia A, Eleonori R, Maponi P, Rossi R, Murri R. MR Imaging and Osteoporosis: Fractal lacunarity analysis of trabecular bone. IEEE Transactions on Information Technology in Biomedicine. 2006;10(3):484–489.

[36] Kiselev V, Hahn K, Auer D. Is the brain cortex a fractal? Neuroimage. 2003;20:1765–1774.

[37] Russell D, Hanson J, Ott E. Dimension of strange attractors. Physical Review Letters. 1980;45(14):1175–1178.

[38] Kilic K, Abiyev R. Exploiting the synergy between fractal dimension and lacunarity for improved texture recognition. Signal Processing. 2011;91:2332–2344.

[39] Nekka F. On lacunarity analysis. In: Fractals in Biology and Medicine. vol. 3; 2002.

[40] IBSR; Available from: http://www.cma.mgh.harvard.edu/ibsr/.

[41] AANLIB; Available from: http://www.med.harvard.edu/aanlib/.

[42] BrainWeb; Available from: http://www.bic.mni.mcgill.ca/brainweb/.

[43] Puspitasari F, Volkau I, Ambrosius W, Nowinski W. Robust calculation of the midsagittal plane in CT scans using the Kullback-Leibler's Measure. Int J CARS. 2009;4:535–547.

[44] Schabel M. 3D Shepp Logan Phantom;. Available from: http://www.mathworks.com/.

[45] Sarkar N, Chaudhuri B. An Efficient Differential box-Counting approach to compute fractal dimension of image. IEEE Transactions on Systems, Man and Cybernetics. 1994;24(1):115–120.

[46] Stegmann M, Skoglund K, Ryberg C. Mid-sagittal plane and mid-sagittal surface optimization in brain MRI using a local symmetry Measure. In: The proceedings of SPIE. vol. 5747; 2005. p. 568–579.

[47] Lee S, Liu Y. Curved glide-reflection symmetry Detection. IEEE Transactions on Pattern Analysis and Machine Intelligence. 2012;34(2):266–278.

[48] Kuijf H, Viergever M, Vincken, K. Automatic extraction of the curved midsagittal brain surface on MR images. MCV 2012 LNCS 2013; 7766: 225-232.
[49] Rorden C, Brett M. Stereotaxic display of brain lesions. Behavioural Neurology. 2000;12:191–200.
[50] Romanesco; 2004. Available from: http://pdphoto.org/.
[51] Lazebnik S, Schmid C, Ponce J. A sparse texture representation using local affine regions. IEEE Transactions on Pattern Analysis and Machine Intelligence. 2005;27(8):1265–1278.
[52] IDOLON; Available from: http://web2.wzw.tum.de/dvs/idolon/.

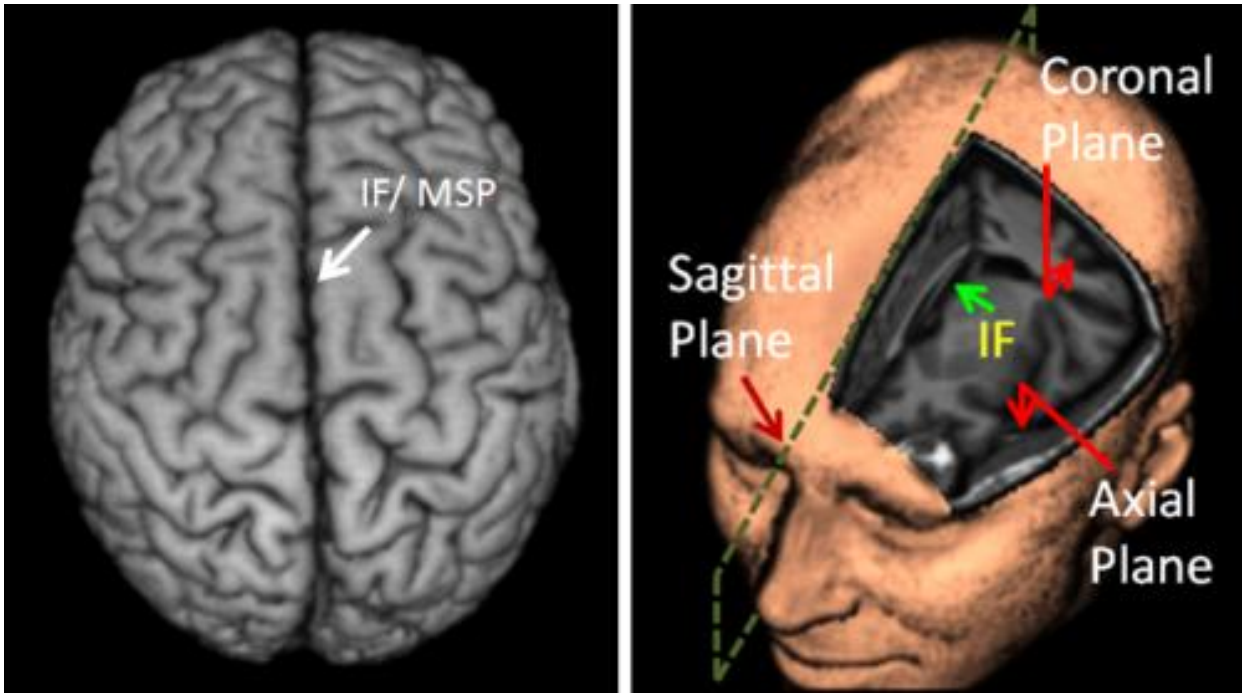

Fig. 1. Mid-sagittal plane [49]

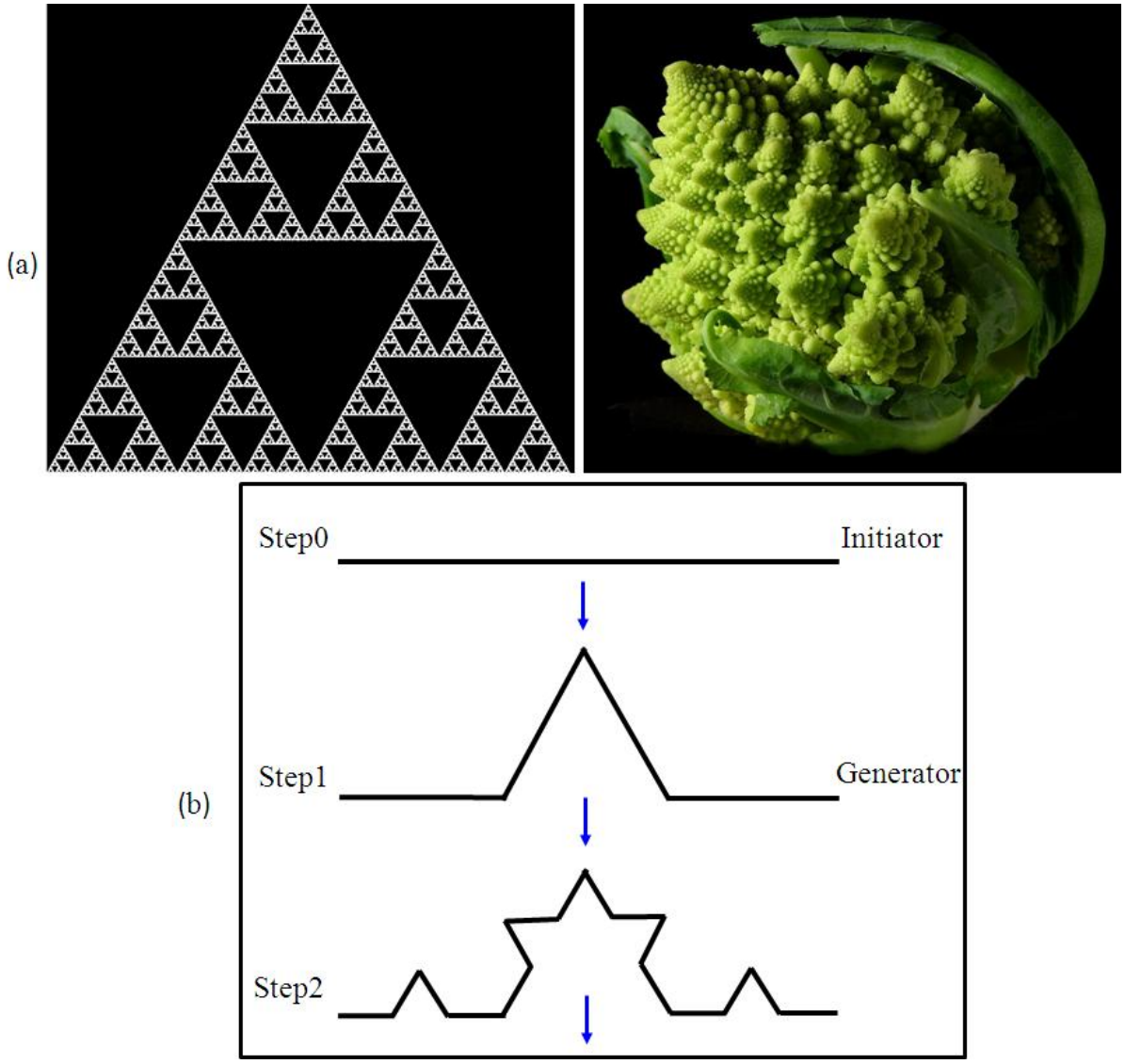

Fig. 2. Examples of fractals. (a). Left: An example of a mathematical fractal, Sierpinski Triangle. Right: An example of a fractal in nature, Romanesco Broccoli [50].
(b). The simple geometric construction of the Koch curve

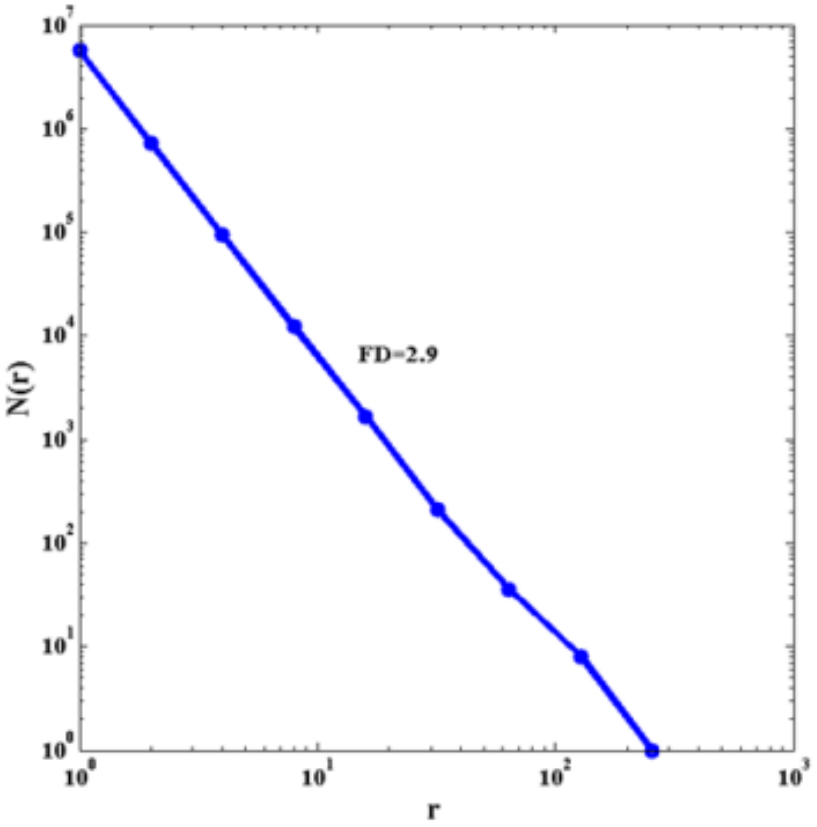

Fig 3. Experiments for the validation of the method. (a) Log-log plot of a 3D brain MRI. It does show some linearity within some range of scale.

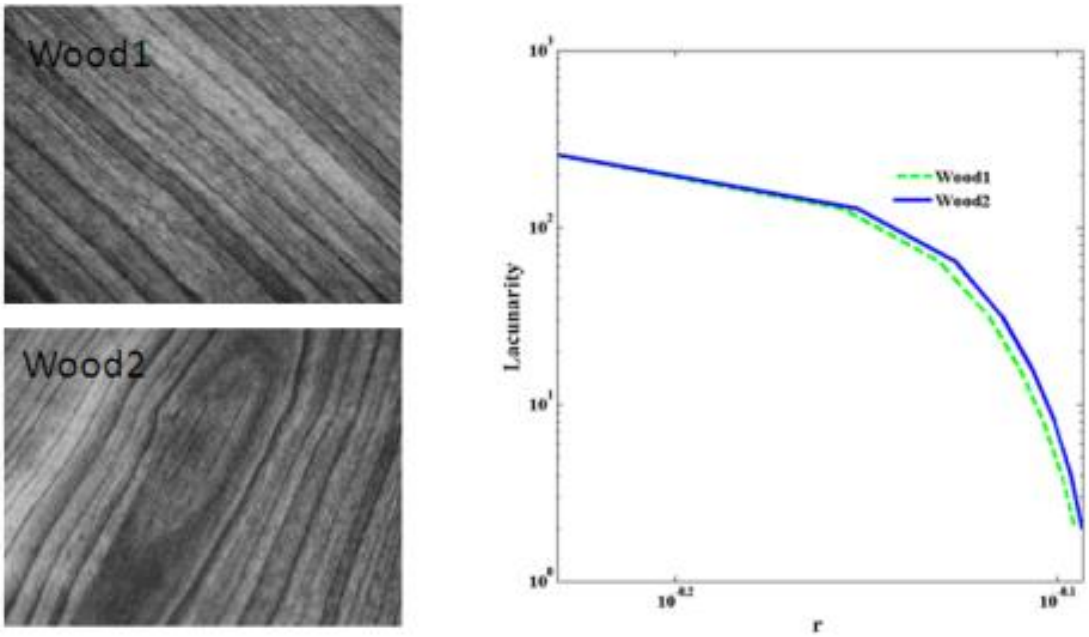

Fig 4. Lacunarity plots of two textural images taken from UIUC database [51]

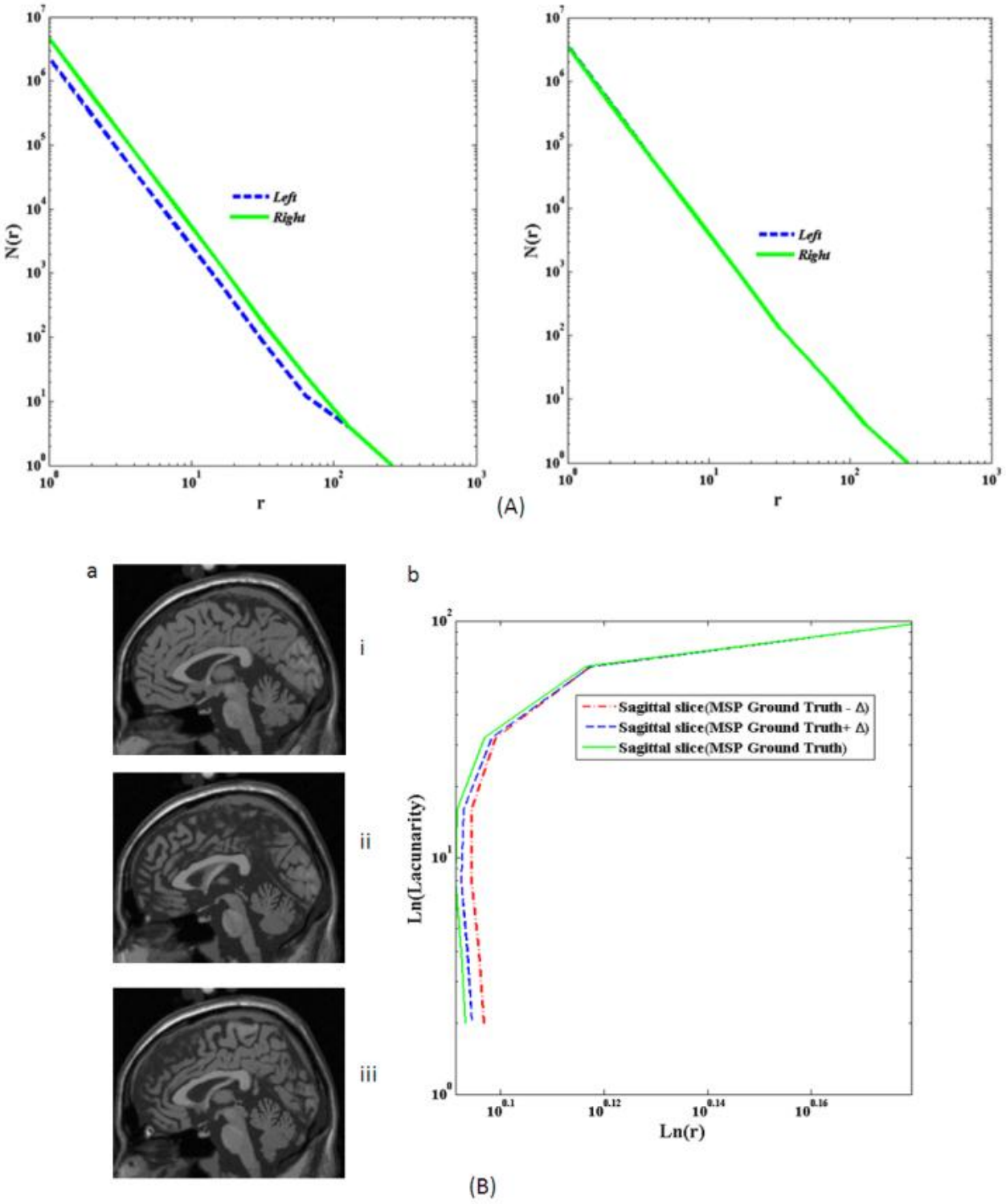

Fig. 5. Validation of the methodology. (A). FD of left-right parts of the brain. Left: Divided at a random sagittal location. Right: Divided at MSP ground truth.
(B). (a) (i) Sagittal slice left to MSP. (ii) Sagittal slice at MSP. (iii). Sagittal slice right to MSP. (b) Lacunarity value of MSP ground truth and two immediate neighbouring slices.

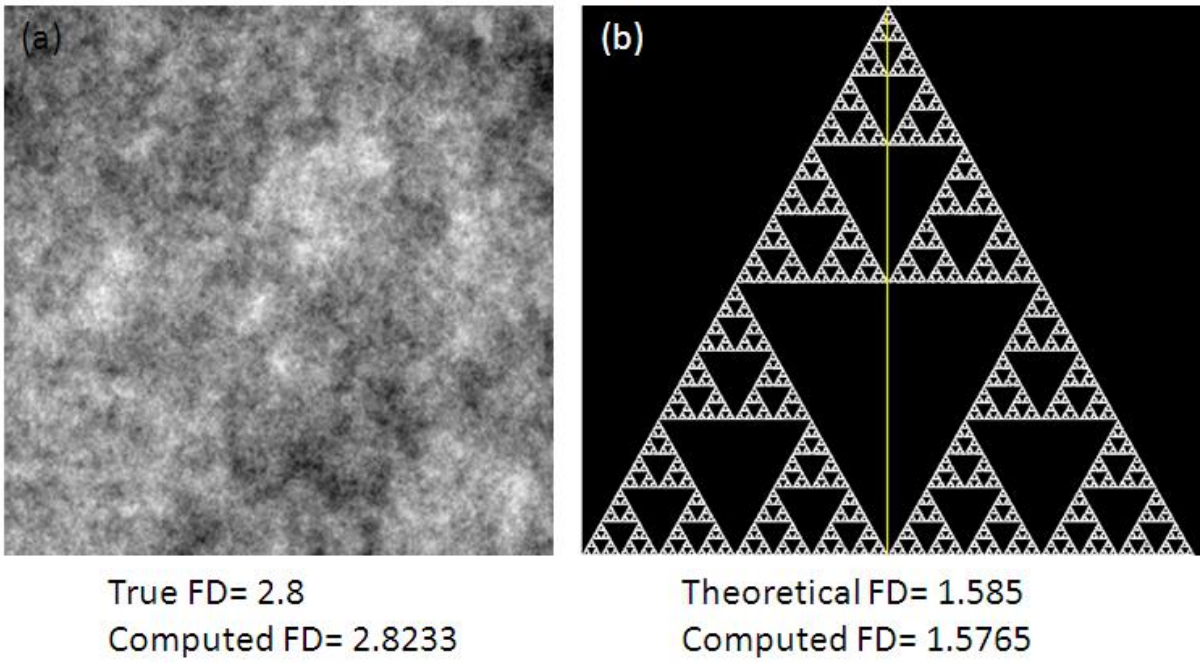

Fig. 6. Experiments for the validation of our method. (a) Fractal dimension computed using the box-counting algorithm on an artificially generated fractal image [52]. (b) Validation of the fractal symmetry detection method on the Sierpinski triangle.

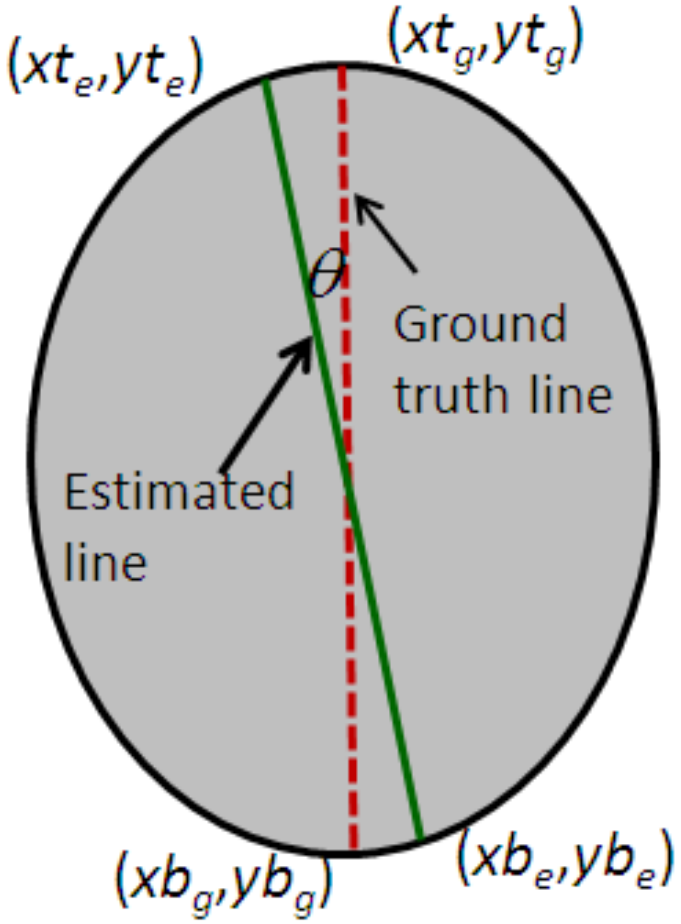

Fig. 7. Calculation of the deviation with the ground truth.

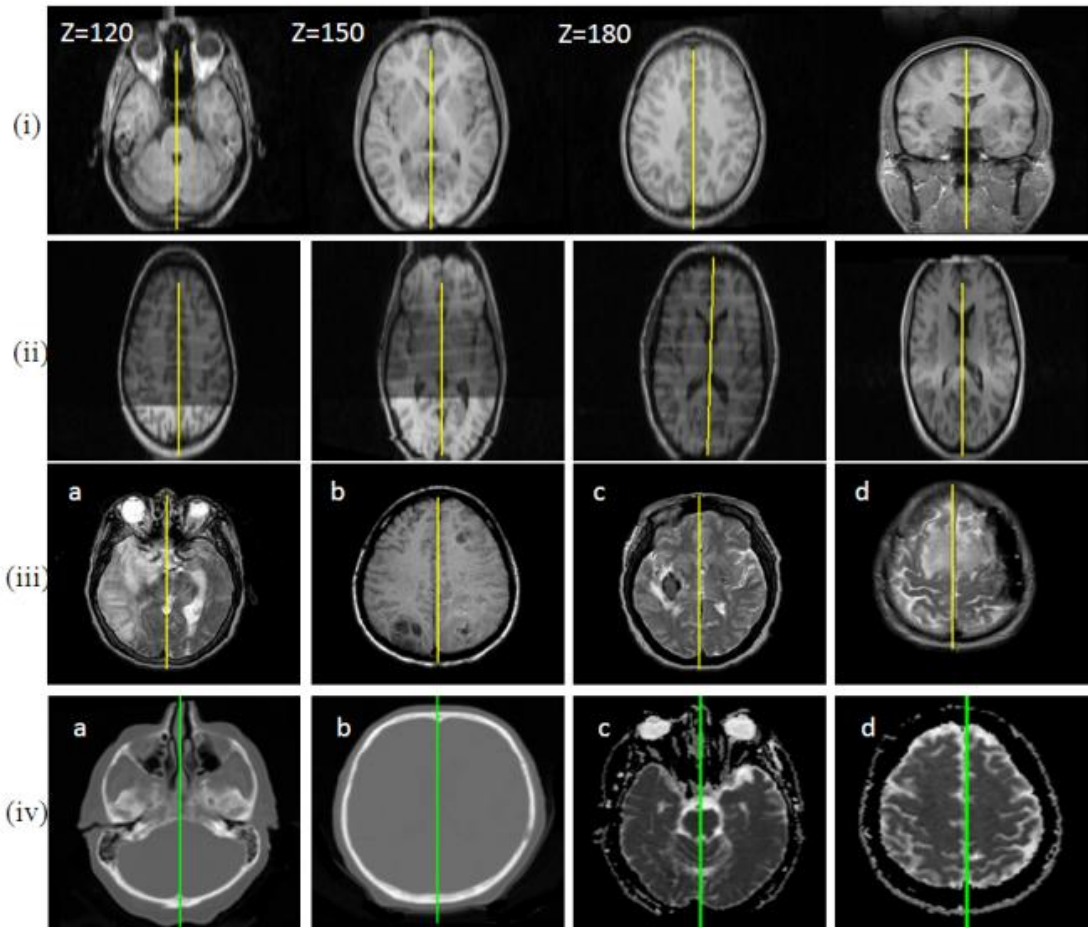

Fig.8. Estimated MSPs projected at axial/ coronal slices. (i). A single image at different axial locations and a coronal slice. (ii). Normal brain images taken from different subjects. (iii). Pathological images. (a). Stroke. (b).Sarcoma. (c).Haemorrhage. (d). Meningioma. (iv). Tested also on CT (a and b) and DWI (c and d).

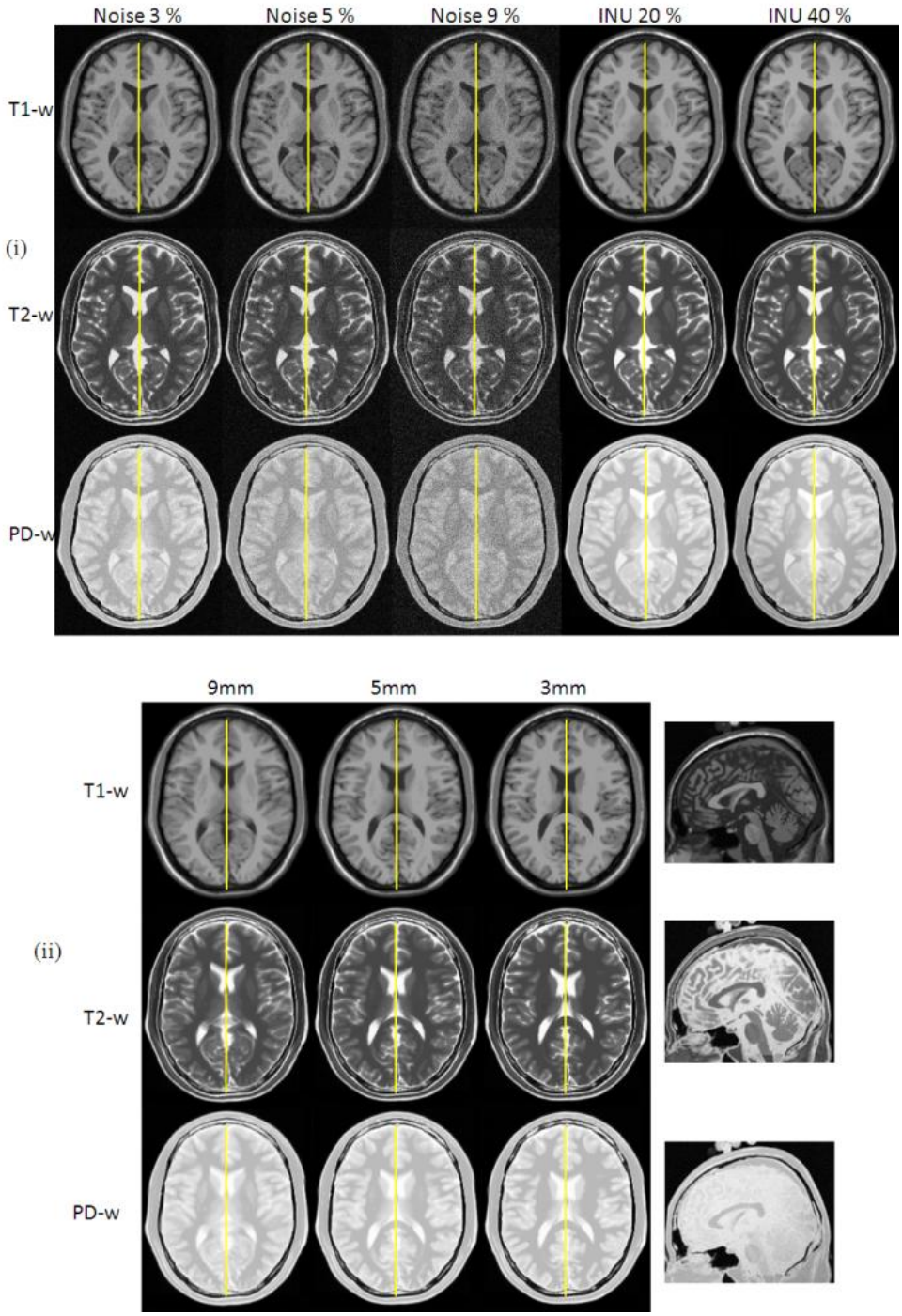

Fig.9. Performance on simulated images. (i). MSPs projected at axial slices using simulated images from BrainWeb with various noise, INU, and modality. (ii). MSPs projected at axial slices with varying slice thickness and modality.

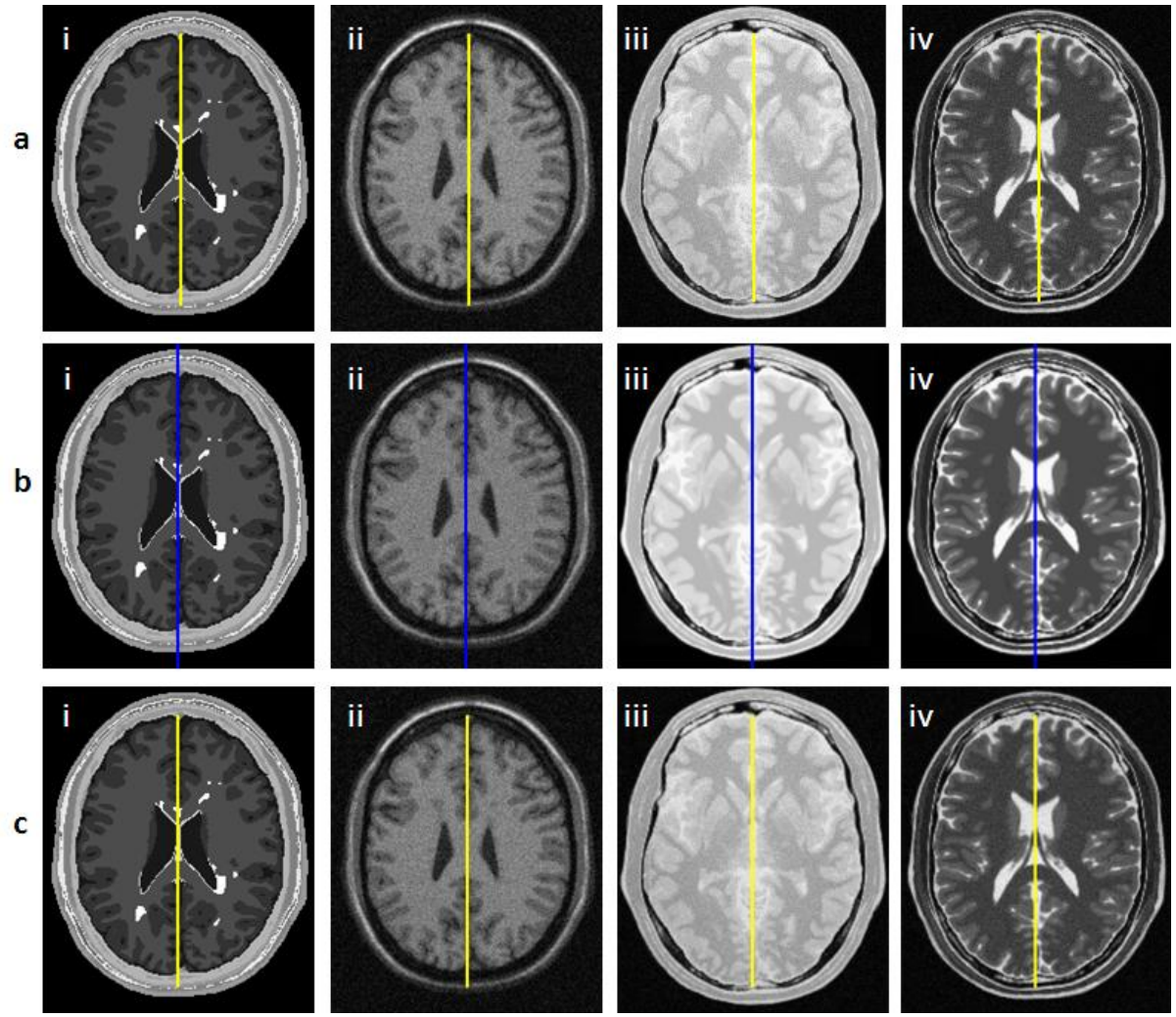

Fig. 10. Comparison with the current state-of-the-art techniques. (a)Our method. (b)cross-correlation technique. (c)KLD technique. (i)MS Lesion. (ii)Noise 9%. (iii)PDW. (iv)T2.

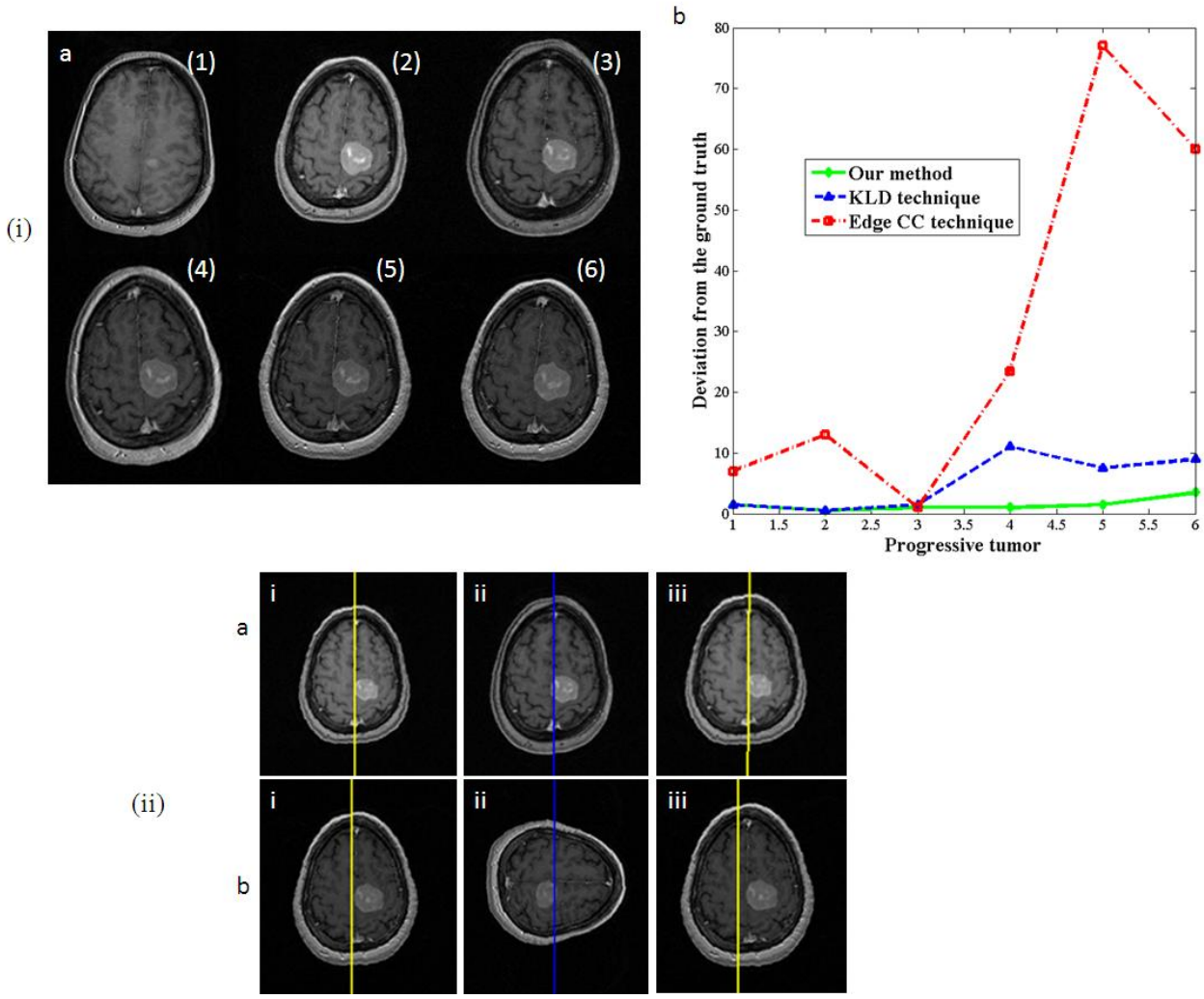

Fig.11. Performance on pathological images. (i). Deviation with the ground truth with the progressive tumor. (a).Tumor images considered. (b). Deviation with the ground truth. (ii). Performance on tumor images. (a).Best performed image of each method. (b).Least performed image of each method.
(i).Our method. (ii). Edge cc method. (iii). KLD method.

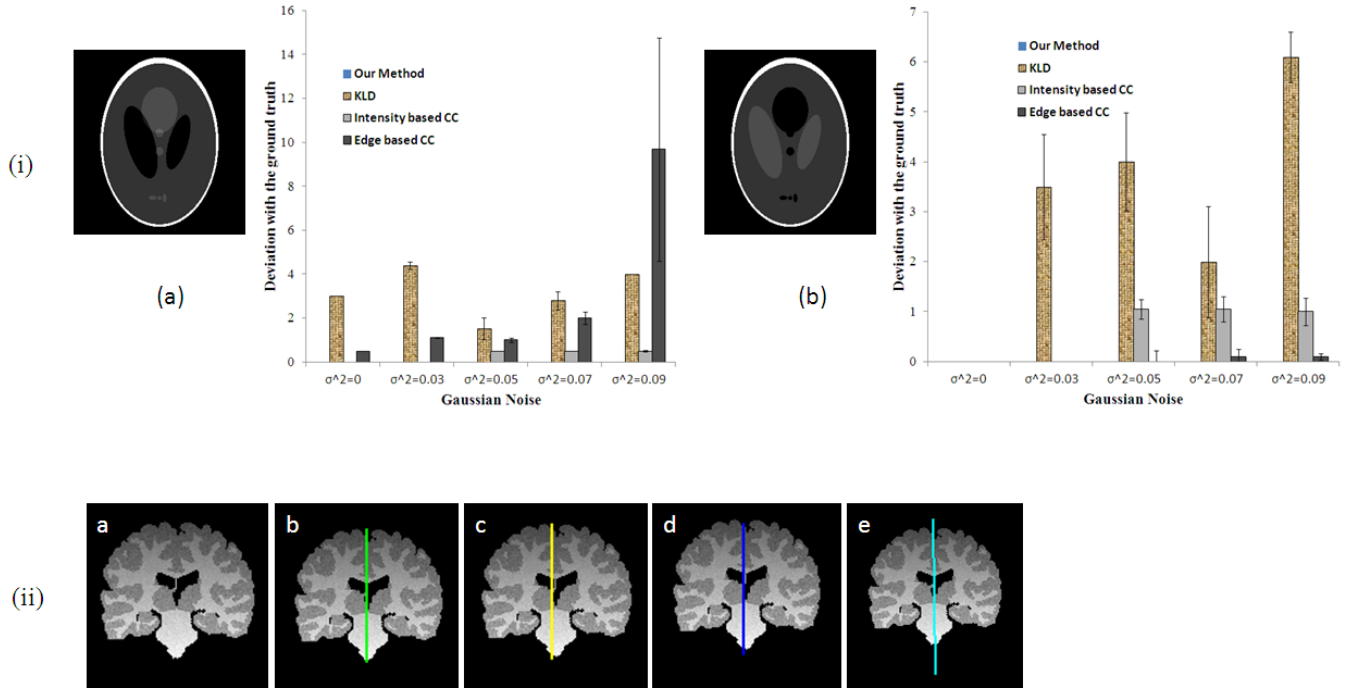

Fig. 12. Experiments for noise on phantom images. (i). Deviation from the ground truth with varying noise. (a)Shepp-Logan image. (b)Contrasts changed in the Shepp-Logan image. (ii). Performance on a phantom brain image. (a). Phantom brain image. (b)Our method. c)KLD method. d)Edge based cc method. e) Intensity based cc method.

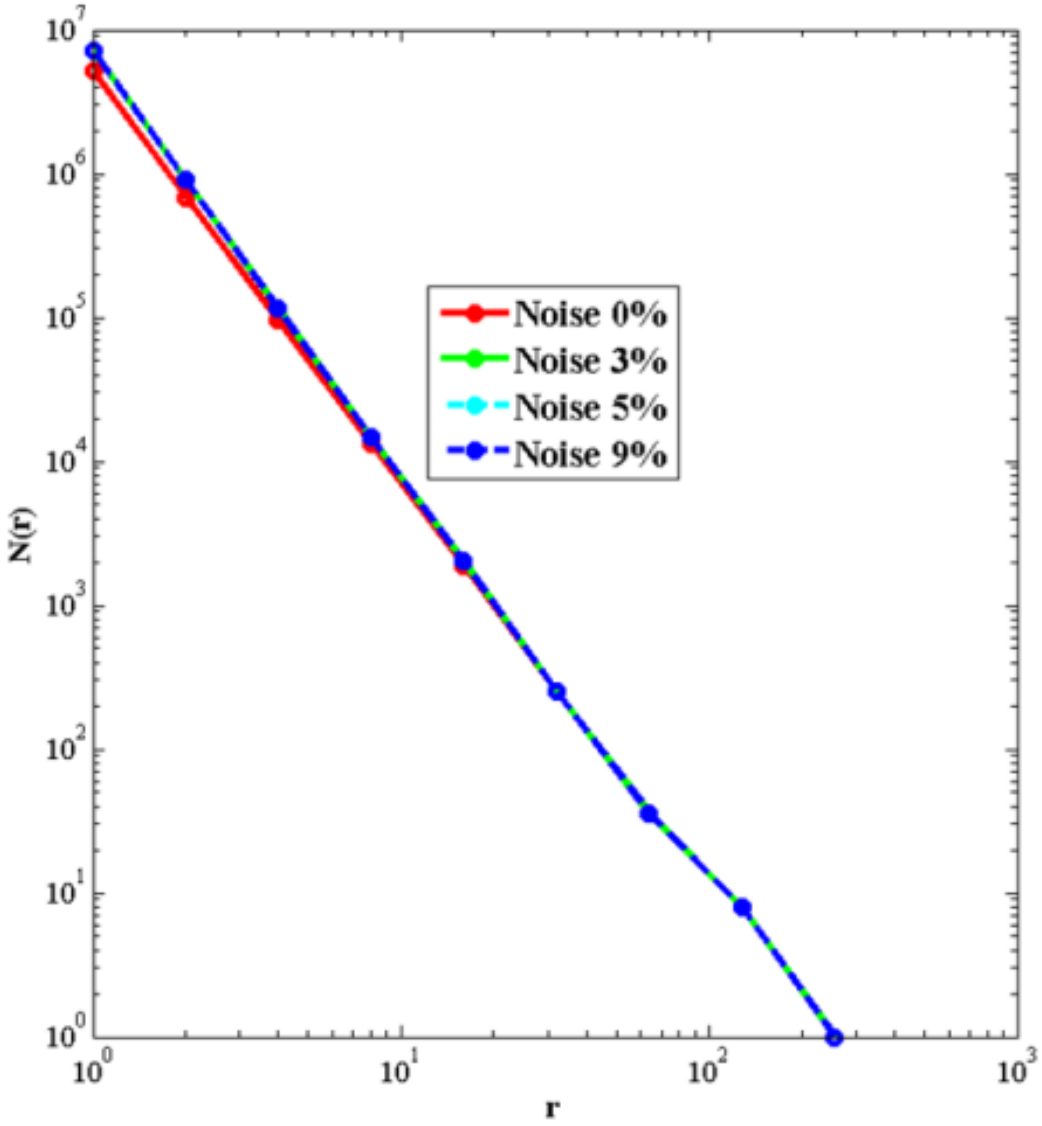

Fig. 13. Log-log plots of BrainWeb Images with varying noise

Table 1. Description of the data sets used

Data source	Number of images	Remarks
IBSR	53	Ground truth was available for 38 images. This dataset was used for quantitative analysis shown in Table 2
AANLIB	08	Ground truth was available for 4 images. These images were used for analysing the effect of a range of pathologies.
BrainWeb	43	Ground truth was available for all images. These datasets were used to analyse the effect of noise, INU, slice thickness, and rotation. Summary of these results is shown in Table 3.
Clinical data	36	Ground truth was not available. These images were used to test the applicability of the method, and were visually assessed by a medical doctor.

Table 2. Difference of our method with the ground truth

θ (in degrees)		**d (in pixels)**	
mean	stdev	mean	stdev
0.08	0.1	0.6	0.26

Table 3. Comparison with the existing work*

	d_{mean}	d_{stdev}	Average computational time
Our method (FD only)	0.41	0.19	2 min
Our method (refined using λ)	0.22	0.25	3 min
Edge CC method	0.54	0.19	8 min
KLD method	0.52	0.12	8 sec

Table 4. Results of the paired t-test

	FD only *t*-value	FD only *p*-value	With λ *t*-value	With λ *p*-value
With Edge CC method	3.020	0.0048	3.730	0.001
With KLD method	3.187	0.003	4.221	0.0002